ON THE USE OF TIME-DOMAIN SAR FOCUSING IN SPACEBORNE SAR MISSIONS

Marc Rodriguez-Cassola, Pau Prats-Iraola, Gerhard Krieger, Alberto Moreira

Microwaves and Radar Institute, German Aerospace Center (DLR)

ABSTRACT

This paper discusses the relevance and use of efficient focusing in the time domain in spaceborne SAR. With the increasing number of space-variant corrections required by higher resolution and wide swath observations, the efficiency of SAR focusing algorithms in the Fourier domain drops significantly. The main sources of space variance to be faced in future spaceborne SAR missions and their implications on the complexity of the focusing process are discussed. The paper also presents a direct comparison between time-domain and frequency-domain approaches, providing an estimate of the computational burden of a fast-factorized backprojection algorithm compared to a sophisticated numerical ωk, identifying the operation areas where the the former may show an efficiency advantage.

Index Terms— SAR processing, fast-factorized backprojection, numerical ωk, spaceborne SAR.

1. INTRODUCTION

The assumption of system and geometrical invariance over wide areas has held in a reasonable manner in conventional spaceborne surveys, leading almost inevitably to the use of SAR focusing schemes in the Fourier domain. Nonetheless, improvements in performance or observation diversity provided by future SAR missions are expected to have a relevant impact on this invariance assumption, opening a window of opportunity to the use of efficient focusing techniques in the time domain.

Besides an *exact* accommodation of space-variant effects, time-domain SAR focusing techniques provide a number of additional advantages to the ground segment system engineer. In the first place, the ability of processing the images on a geocoded grid, which might reduce access costs for future users. And secondly, the availability of a generic processing kernel, valid for wide-band monostatic and bistatic geometries, both squinted and non-squinted, almost independent of the imaging mode, especially interesting for prototyping and simulation environments. Further advantages, particularly relevant for squinted or steered observations, encompass the natural accommodation of time and frequency folding.

We aim in this paper at discussing the relevance of efficient time-domain focusing techniques in operational environments for future SAR missions. In particular, it will be shown that the modulation parameters and the effective antenna pattern with which targets are illuminated in reflector- and scan on receive based systems change with topography (for specific areas) in such a way that the computational complexity of Fourier-based algorithms may equal or exceed that of efficient time-domain ones, provided the resolution is approaching 10λ.

The paper is divided as follows. Section 2 presents two canonical and comparable versions of efficient time-domain and Fourier-domain algorithms, including a critical discussion concerning computational burden and accuracy. Section 3 presents a description of the sources of space variance in spaceborne SAR and quantifies the impact of topography on the efficiency of the canonical Fourier-based algorithm presented in Section 2. Section 4 ends the paper with a discussion.

2. EFFICIENT TIME-DOMAIN VERSUS FOURIER-BASED: A CRITICAL VIEW

As sufficiently recognized in the available literature [1, 2], efficient time-domain SAR focusing algorithms are typically based on a divide-and-conquer strategy and achieve logarithmic burden reductions by minimizing the number of image samples and reducing the cost of intermediate interpolations. In this manner, the computational burden of building a synthetic aperture being $\mathcal{O}(N^2)$ is relaxed by coherently -and smartly- adding the images of smaller subapertures. Due to its advantageous intermediate geometries, the archetype of efficient SAR focusing algorithms in the time domain is the fast-factorized backprojection, acronymed FFBP in the literature [2]. In the general case where N is a power of M, the simplified computational complexity of FFBP running through K stages becomes $M^K \cdot \mathcal{O}(M^{2\cdot(P-K)})$, with $P = \log_M N$.

In theory, FFBP could be factorized to the limit of building M-pulse subapertures, achieving the usual efficiency gain of the canonical Fourier-based SAR image formation kernels. In practical terms, however, this is usually not the case, and the factorization is stopped to a minimum subaperture to prevent aliasing at lower resolution stages. It is perhaps worth stating that Fourier-based kernels face analogous -though not

Table 1. Computational burden FFBP run through K stages

Range compression (RC)	$\mathcal{O}(2 \cdot \log_2 N_\mathrm{r} + 1)$
Backprojection (DBP)	$\mathcal{O}((M_\mathrm{r} + 2) \cdot 2^{\log_2 N_\mathrm{a} - K})$
Grid computation	$\mathcal{O}(3 \cdot K)$
Interpolation	$\mathcal{O}(K \cdot M_\mathrm{r} \cdot M_\mathrm{a})$

necessarily comparable- drops in efficiency whenever a zero-padding for efficiency reasons (e.g., to the next friendly power of M) is effected.

Table 1 shows a rough estimate of the computational burden -measured as number of complex multiplications- of the main steps of FFBP run through K stages, all normalized by the number of samples of the data block, where N_r and N_a are the number of samples in range and azimuth, respectively, and M_r and M_a are the length of the interpolation kernels, all effected in the time domain. We believe it pertinent to clarify the assumptions of the analysis: i) N_a has been assumed to be a power of two, ii) the burden in the evaluation of the processing functions has been been asssumed to be negligible compared to the overall cost of the algorithms, and iii) any systemic polychromatic corrections have been ignored since they are expected to increase the burden of both approaches in a similar way. These assumptions, especially the former, are thought to favorise the ωk kernel over the FFBP, and shall be critically discussed in the final version of the paper. Specifically concerning Table 1, the factor $M_\mathrm{r} + 2$ in the burden of DBP corresponds to the compensation of radiometric and phase components and interpolation of the range compressed echoes. Note that the accurate consideration of the orbital geometry suggests that the computation of the grid at every factorization step cannot rely on the approximation of a slant range plane. Fortunately enough, this computation can be effected in a smart way without requiring a dedicated back-geocoding at every factorization step, and can be substituted in practical terms by a linear interpolation, as discussed in the bistatic version of the algorithm in [3].

For the sake of comparison, the Fourier-based algorithm suggested in [4] is used. The structure of the algorithm in [4] replicates a numerical ωk based on a SVD factorization [5], with additional residual range cell migration and azimuth compression steps. For space-variant corrections, motion compensation (e.g., implemented using SATA or PASTA) capabilities as described in [6] have been added. As in the case of FFBP, the algorithm is capable of handling high-resolution, monostatic and bistatic surveys, with large squints, while offering space-variant correction skills. A rough estimate of the computational burden is shown in Table 2, again normalized by the size of the data block. The three assumptions listed above are maintained in the analysis. M_r is the length of an interpolation kernel in the time domain, corresponding to the range interpolation and cell migration correction in the range-Doppler domain, and m_r the length of an interpolation

Table 2. Computational burden ωk

2D DFT	$\mathcal{O}(\log_2 N_\mathrm{r} + \log_2 N_\mathrm{a})$
Bulk focus	$\mathcal{O}(2)$
Range cell migration correction (RCMC)	$\mathcal{O}(M_\mathrm{r} + m_\mathrm{r} + 3)$
Residual correction (AC + RCMC)	$\mathcal{O}(M_\mathrm{r} + 3)$
2D iDFT	$\mathcal{O}(\log_2 N_\mathrm{r} + \log_2 N_\mathrm{a})$
Space-variant corrections (MoCo)	$\mathcal{O}(k \cdot (2 \cdot \log_2 M_\mathrm{a} + M_\mathrm{r} + 3))$

kernel in the frequency domain, corresponding to the Stolt mapping. We differentiate between both to foresee the use of larger kernels in the frequency domain. The value of M_a shows the number of samples used in the space-variant correction (MoCo) windows, which controls the resolution of these corrections, whereas the k is a factor controlling the overlap. If SATA is considered, k takes a value of 2; using PASTA would increase the value of k by a factor inversely proportional to the number of valid samples after the correction. Note the term M_r in the MoCo burden assumes a residual space-variant range cell migration is corrected. The 3 found at different stages are due to cubic interpolations of azimuth compression and range cell migration kernels along the swath.

The burden of the algorithm is shared among the Stolt mapping, the bulk focus and the space-variant corrections. Fig. 1 shows the relative burden according to Tables 1 and 2 for a FFBP implementation with 12-point interpolation kernels in both range and azimuth and a minimum subaperture size of 32 samples and an ωk implementation using 64-point kernels at Stolt mapping and including 64-point space-variant correction windows based on SATA (e.g., $k = 2$). The figure has been computed with 120 k-samples in range, but changes little with N_r as expected from the expressions in the tables.

The values shown in the figure are indeed exemplary, but represent accurate implementations of the algorithms and quantify the trade-off between space-variance capabilities and spectral purity. FFBP is able to provide sample-wise corrections but accumulates aliasing -in form of interpolation errors- through all its stages, expected to show as a raise in ISLR of the impulse response of the system [7]. On the other hand, ωk provides aliasing-free data but with space-variant corrections with coarser resolution.

3. TOPOGRAPHY AS MAIN SOURCE OF SPACE VARIANCE IN SPACEBORNE SAR

As discussed in the literature [8], there exist several sources of space variance in spaceborne surveys, which can be mainly classified as geometrical, atmospheric and systemic, includ-

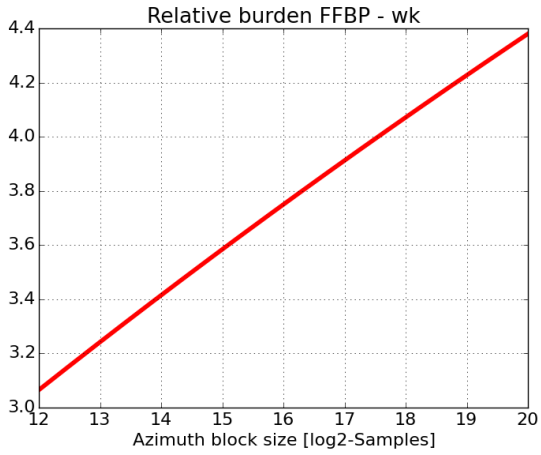

Fig. 1. Relative burden between the reference FFBP and the ωk implementation according to Tables 1 and 2. The FFBP implementation uses 12-point interpolation kernels in range and azimuth and has a minimum subaperture size of 32 samples. The ωk implementation uses 64-point kernels for the Stolt mapping and provides SATA-based space-variant corrections using windows with 64 samples.

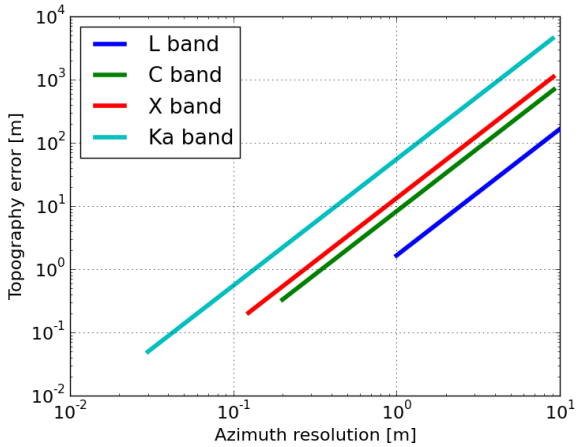

Fig. 2. Maximum height deviation which can be tolerated at focusing stages to keep the interferometric error below 10 deg as a function of the azimuth resolution and frequency band for a LEO system flying on a 514 km orbit.

ing aspects such as scene topography, orbit and attitude control, orbit eccentricity, Earth rotation, tropospheric and ionospheric propagation, imaging mode and steering, instrument and spacecraft stability, etc.

Of all elements presented above, topography shows the highest spatial rate of change, which makes it the obvious candidate to assess the pertinence of using FFBP in a spaceborne operational scenario.[1] The analysis is conducted by considering phase and amplitude errors intrinsically due to topographic variations as caused by changes in the effective velocity of the survey and the antenna pattern on ground. Assuming a maximum tolerable error of ϵ_ϕ in the interferometric phase, the maximum topographic variation which can be tolerated within the correction block can be expressed as [9]

$$\delta h \leq \frac{v_{\mathrm{e}} \cdot \delta x^2}{\lambda \cdot r_0 \cdot f_{\mathrm{v}}} \cdot \frac{\epsilon_\phi}{3\pi} \quad , \tag{1}$$

where λ is the carrier wavelength, r_0 is the slant range, v_{e} is a reference effective velocity in the survey, δx is the azimuth resolution, and f_{v} is the sensitivity of the effective velocity with topography. Fig. 2 shows the values of (1) for a phase error of 10 deg and different values of azimuth resolution and frequency bands for a LEO system flying on a 514 km orbit. The tolerance with respect to topographic errors for the same target resolution increases for decreasing frequency bands due to the longer integration times. An approximated value of the number of samples required for the space-variant correction can be expressed as

$$\begin{aligned} M_a \approx & \mathcal{Q}\left[\frac{\delta x}{\delta h} \cdot \frac{\partial h_{\mathrm{DEM}}}{\partial x} \cdot N_{\mathrm{sa}}\right] \\ \approx & \mathcal{Q}\left[\frac{3\pi \cdot f_{\mathrm{v}} \cdot \lambda^2 \cdot r_0^2}{\delta x^3 \cdot v_{\mathrm{e}} \cdot \epsilon_\phi} \cdot \frac{\partial h_{\mathrm{DEM}}}{\partial x}\right] \quad , \end{aligned} \tag{2}$$

where the partial derivative represents the azimuth gradient of the scene topography, N_{sa} is the length in samples of the synthetic aperture, and $\mathcal{Q}[\cdot]$ is a truncation function. Fig. 3 shows (2) without truncation evaluated for a unitary gradient for the same cases of the figure above. We remind the reader to keep in mind the different integration times for a common target resolution for different frequency bands. Note too that the smaller values would truncate to zero in a real situation. Furthermore, the curves scale linearly with the corresponding gradients within the processing block.

Assuming the conditions under which Fig. 1 has been derived, increases of the subaperture sizes of roughly a factor four may be considered as a valid threshold between the ωk and FFBP. In order to get a flavor of the importance of this effect, Fig. 4 shows two topography gradient maps over Barcelona (top) and the eastern side of West Kalimantan, in Borneo (bottom). The gradients are likely optimistic, since they have been computed using SRTM data. The situation described by Fig. 3 would be improved in the Barcelona case and roughly maintained, if not worsened, in the Bornean case.

A further consequence of topography is the variance of the effective antenna patterns with which the different parts of the scene are observed. A modulation in amplitude -and

[1] We acknowledge that propagation effects may also show strong spatial bandwidths in turbulent scenarios. However, they may not be known a priori and therefore not considered in the current work as subject of compensation.

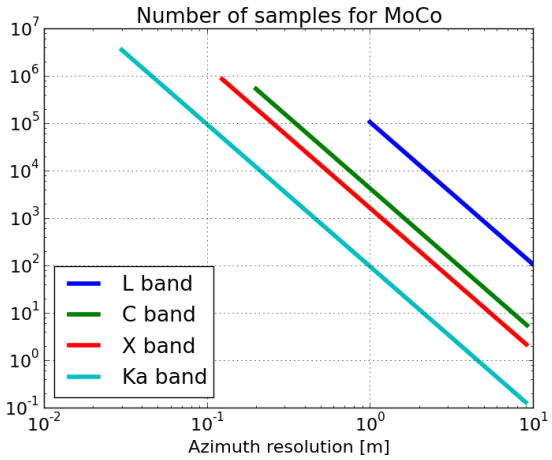

Fig. 3. Approximate number of samples required for the space-variant corrections in the ωk assuming a unitary topography gradient and as a function of the wavelength and the azimuth resolution.

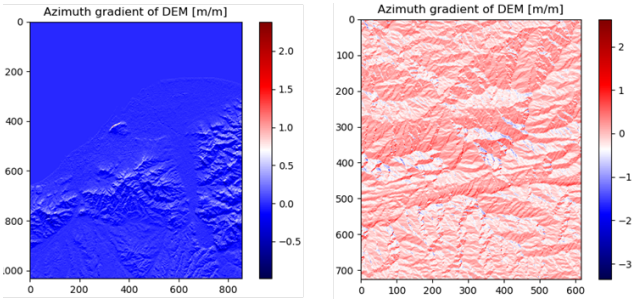

Fig. 4. Topography azimuth gradient maps computed using SRTM data over Barcelona (top) and West Kalimantan, Indonesia (bottom).

phase- appears in the case of non-separable antenna patterns (e.g., reflector-based) and planar array systems working with scan on receive (SCORE), provided the SCORE coefficients are varying with time. In the final version of the paper, the analysis shall be refined and completed by incorporating the impact of the antenna patterns.

4. SUMMARY

The paper has presented a critical discussion of the oportunities for fast backprojection algorithms in operational spaceborne SAR scenarios. The analysis, which needs to be refined and completed for the final version of the paper by incorporating the impact of the spatial variability of the antenna patterns, shows FFBP may have an efficiency edge for high-resolution systems.

5. REFERENCES

[1] A. F. Yegulalp, "Fast backprojection algorithm for synthetic aperture radar," in *Proc. IEEE Radar Conference*, Waltham, USA, Apr. 20-22, 1999, pp. 60–65.

[2] L. Ulander, H. Hellsten, and G. Stenström, "Synthetic aperture radar processing using fast factorized back-projection," *IEEE Trans. Aerosp. Electron. Syst.*, vol. 39, no. 3, pp. 760–776, Jul. 2003.

[3] M. Rodriguez-Cassola, P. Prats, G. Krieger, and A. Moreira, "Efficient time-domain image formation with precise topography accommodation for general bistatic SAR configurations," *IEEE Trans. Aerosp. Electron. Syst.*, vol. 24, no. 3, pp. 218–223, Oct. 2011.

[4] P. Prats-Iraola, M. Rodriguez-Cassola, and A. Moreira, "Investigations on bistatic SAR image formation for the SAOCOM-CS mission," in *Proc. EUSAR*, Hamburg, Germany, Jun. 2–5, 2016, pp. 1–4.

[5] D. D'Aria and A. Monti Guarnieri, "High-resolution spaceborne SAR focusing by SVD-Stolt," *IEEE Geosci. Remote Sens. Lett.*, vol. 4, no. 4, pp. 639–643, Oct. 2007.

[6] P. Prats-Iraola, M. Rodriguez-Cassola, R. Scheiber, and A. Reigber, "Accommodation of space-variant effects in spaceborne SAR image formation," in *Proc. IGARSS*, Quebec, Canada, Jul. 21–25, 2014.

[7] P.-O. Frölind and L. Ulander, "Evaluation of angular interpolation kernels in fast back-projection SAR processing," *IEE Proc. Radar Sonar Navig.*, vol. 153, no. 3, pp. 243–249, Jun. 2006.

[8] M. Rodriguez-Cassola, P. Prats-Iraola, R. Scheiber, and A. Moreira, "Geometrical considerations of spaceborne SAR surveys," in *Proc. EUSAR*, Berlin, Germany, Jun. 2–5, 2014, pp. 1–4.

[9] M. Rodriguez-Cassola, P. Prats-Iraola, F. De Zan, R. Scheiber, A. Reigber, D. Geudtner, and A. Moreira, "Doppler-related distortions in TOPS SAR images," *IEEE Trans. Geosci. Remote Sens.*, vol. 53, no. 1, pp. 25–35, Jan. 2015.